Published for SISSA by Springer

Received: December 12, 2025
Accepted: December 30, 2025
Published: February 18, 2026

Three-loop corrections to $gg \to ZH$ in the large top quark mass limit

Joshua Davies[a], **Dominik Grau**[b], **Kay Schönwald**[c], **Matthias Steinhauser**[b] and **Daniel Stremmer**[b]

[a] *Department of Mathematical Sciences, University of Liverpool, Liverpool, L69 3BX, U.K.*
[b] *Institut für Theoretische Teilchenphysik, Karlsruhe Institute of Technology (KIT), Wolfgang-Gaede Straße 1, 76131 Karlsruhe, Germany*
[c] *Physik-Institut, Universität Zürich, Winterthurerstrasse 190, 8057 Zürich, Switzerland*

E-mail: J.O.Davies@liverpool.ac.uk, dominik.grau@kit.edu, kay.schonwald@cern.ch, matthias.steinhauser@kit.edu, daniel.stremmer@kit.edu

Abstract: We compute three-loop virtual corrections to the associated production of a Higgs boson with a Z boson in the large-m_t limit. We describe in detail the application of the asymptotic expansion and provide, for all form factors, analytic results for the first three terms in the $1/m_t$ expansion. We also provide numerical routines implemented in the `C++` library `ggxy`.

Keywords: Higgs Production, Higher-Order Perturbative Calculations

ArXiv ePrint: 2512.00156

https://doi.org/10.1007/JHEP02(2026)191

JHEP02(2026)191

Contents

1 Introduction

The associated production of a Higgs boson with a vector boson, $W^{\pm}$ or Z, provides the third-largest cross section for Higgs boson production at the LHC. Furthermore, it is an important process for the measurement of the Higgs coupling to bottom quarks [1–3], which is difficult in other Higgs production processes due to large backgrounds.

For the quark-initiated channel for VH production, the inclusive cross section is known up to next-to-next-to-next-to-leading order ($\mathrm{N^3LO}$) in the strong coupling [4–6] (see also the public code `VH@NNLO` [7, 8] which includes next-to-next-to-leading order (NNLO) corrections). Differential cross sections have been computed in refs. [9, 10] and electroweak corrections are known from refs. [11, 12]. They are implemented in the code `HAWK` [13].

In contrast to WH production, ZH production receives contributions from a gluon-initiated subprocess which has been computed at leading order (LO) in refs. [14, 15]. It comes with a $\mathcal{O}(25)\%$ scale uncertainty which induces a 3% uncertainty [16] on the complete ZH contribution. Although the LO $gg \to ZH$ process is a NNLO contribution to the $pp \to ZH$ cross section, higher-order corrections to $gg \to ZH$ are numerically important. This is particularly true in the boosted regime [17] where the gg-initiated channel gains relative importance with respect to the $q\bar{q}$ channel. In order to reduce the scale uncertainties in ZH production, next-to-leading order (NLO) corrections to $gg \to ZH$ have been computed in several different works. In [18] the infinite-top-mass limit has been applied and in [19, 20] an expansion in $1/m_t$ has been performed. High-energy results have been obtained in refs. [20, 21] and expansions around the forward limit are available from [21, 22]. Numerical results have been obtained in refs. [23] and [24], where in the latter case an expansion in the external masses has been performed. There are various approaches where either numerical results or different expansions are combined in order to cover the whole phase space; in ref. [25] the numerical results from [23] and the high-energy expansion [20], in ref. [26] the forward expansion and the high-energy expansion [20], and in ref. [21] deep expansions around the forward and high energy limits, see also ref. [27].

JHEP02(2026)191

The aim of this paper is to provide a first step towards NNLO for $gg \to ZH$ by computing three expansion terms for the virtual three-loop corrections, in the large m_t limit. Although the radius of convergence is restricted to a relatively small region in phase space, below the $t\bar{t}$ threshold, the large-m_t calculation serves as benchmark for future exact calculations or calculations in other kinematic limits.

In this paper we provide, in particular, the three-loop virtual corrections in the infinite top quark mass limit which is an important ingredient for the construction of approximate NNLO predictions for $gg \to ZH$. An approximation could be constructed in analogy to the approach outlined in ref. [28] for $gg \to HH$, in which exact results are used up to NLO and for the double-real emission at NNLO, and virtual corrections at NNLO are approximated in the infinite top quark mass limit, re-weighted using NLO results.

The remainder of the paper is structured as follows: in the next section we provide details of the asymptotic expansion in $1/m_t$ and briefly discuss the various integral families which appear. Results for the form factors are presented in section 3. We conclude in section 4. In the appendix we describe the implementation of our results in the `C++` library `ggxy` [29].

2 Technical details

We consider the scattering of two gluons in the initial state with momenta q_1 and q_2 into a Higgs and a Z boson with momenta q_3 and q_4. The Mandelstam variables are then given by

$$s = (q_1 + q_2)^2\,, \qquad t = (q_1 + q_3)^2\,, \qquad u = (q_1 + q_4)^2\,, \tag{2.1}$$

where all momenta are incoming. Furthermore we have

$$q_1^2 = q_2^2 = 0 \qquad q_3^2 = m_Z^2\,, \qquad q_4^2 = m_H^2\,. \tag{2.2}$$

The transverse momentum of the final-state particles is given by

$$p_T^2 = \frac{u\,t - q_3^2 q_4^2}{s}\,. \tag{2.3}$$

The (internal) top quark mass is denoted by m_t. In figure 1 we show sample Feynman diagrams for the virtual corrections to $gg \to ZH$ up to three-loop order (NNLO).

We decompose the amplitude for $g(q_1)g(q_2) \to Z(q_3)H(q_4)$ as a linear combination of form factors following ref. [15]; we use the notation of refs. [20, 21] and obtain six independent form factors given by

$$F_{12}^+(t,u),\ F_{12}^-(t,u),\ F_2^-(t,u),\ F_3^+(t,u),\ F_3^-(t,u),\ F_4(t,u)\,, \tag{2.4}$$

see eqs. (34) and (36) of ref. [21] for more details.

In the computation of $gg \to ZH$ we have to take into account the contributions from light and heavy quarks inside the loops. The contributions proportional to the vector coupling vanish exactly. Therefore, only the axial-vector coupling has to be taken into account. Since the axial-vector coupling is proportional to the third component of the weak isospin of the quark $I_{u,d}^3 = \pm 1/2$, the contributions of quark generations with equal masses vanishes.

JHEP02(2026)191

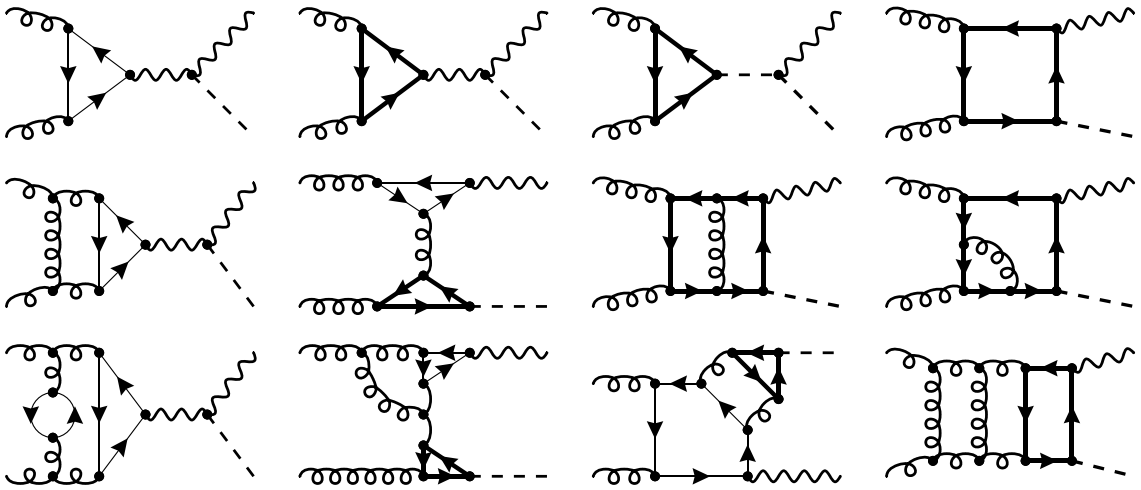

Figure 1. One-, two- and three-loop sample Feynman diagrams contributing to $gg \to ZH$. Solid thin (thick) lines denote massless (massive) quarks. Scalars and gluons are represented by dashed and curly lines, respectively. In the triangle diagrams either a Z boson or Goldstone boson mediates the coupling to the Higgs and Z boson in the final state. At two- and three-loop order both one-particle reducible and one-particle irreducible diagrams have to be considered. These Feynman diagrams were drawn with the help of the FeynGame program [30].

Considering the top quark as the only massive quark, we have to take into account only the axial-vector coupling of the Z boson to top and bottom quarks.

The amplitude is generated with `qgraf` [31] where we encounter 23 diagrams at the one-loop, 398 at the two-loop and 11,866 diagrams at the three-loop level.[1] The output is converted to `FORM` [32] code with the combination of the tools `q2e` and `exp` [33, 34], where the latter tool also performs the mapping to topologies including subgraphs and co-subgraphs as required by the large mass expansion and described in more detail below. Further calculation is then performed with the in-house setup `calc`, where the calculation of the Dirac and colour traces is performed and the amplitude is expanded in the limit of the large top-quark mass. The result is then given as a sum of scalar integrals for which the integration-by-parts (IBP) reduction and insertion of master integrals has to be still carried out.

2.1 Asymptotic expansion

We use `exp` [33, 34] to apply the hard mass expansion procedure (see, e.g., ref. [35]) to the three-loop triangle and box diagrams. This leads to a number of subgraphs and co-subgraphs; see figure 2 for typical examples in graphical from.

In our calculation the following cases appear:

- Three-loop massive subgraph. Here the co-subgraph is a tree-level diagram. For the three-loop vacuum graphs we need tensor integrals up to rank 10.

[1] Goldstone bosons are taken into account and the longitudinal mode of the Z boson is treated as an separate particle.

JHEP02(2026)191

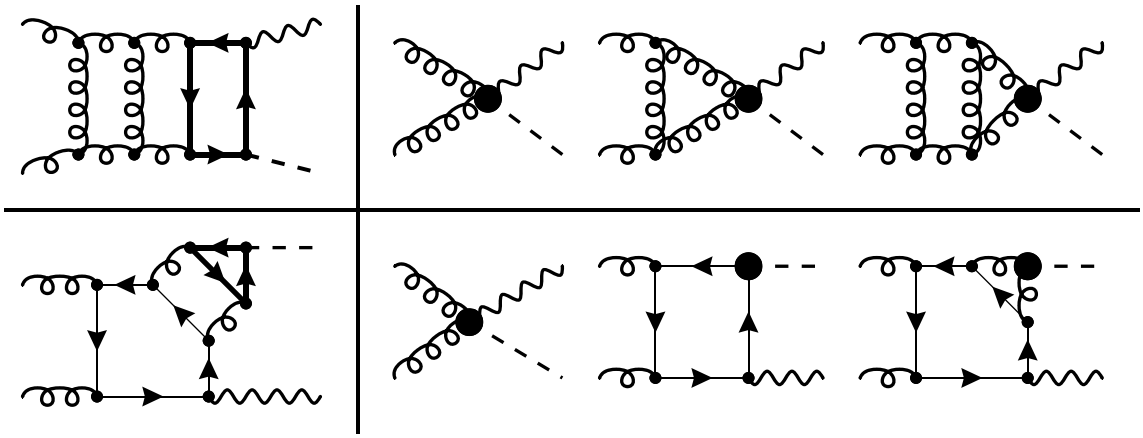

Figure 2. Graphical representation of the asymptotic expansion applied to the diagrams on the left. On the right we show only the co-subgraphs. The corresponding subgraphs are one-, two- and three-loop vacuum integrals which are inserted in the effective vertices represented by the blobs.

- In case the subgraph is a two-loop vacuum integral the co-subgraph is a massless integral with up to four external legs, two of which can be massive (m_H and m_Z). The corresponding integrals are well-known in the literature (see, e.g., ref. [36]).
- The most complicated case is the one where the subgraph is a one-loop vacuum graph. Here the co-subgraph is in general a massless double box integral with two massless legs and two massive legs with masses m_H and m_Z. Below we provide more details about the calculation of this contribution.
- Note that the purely massless diagrams which involve a closed light-quark loop are computed exactly. These are triangle diagrams, where massless form factor integrals are needed.

The main differences to the computation of the large mass expansion of $gg \to HH$ [37] originate from the latter two points, see also diagrams as shown in figure 1. Integral families for two-loop massless box integrals and three-loop massless vertices do not appear for Higgs boson pair production.

One-loop massless box integrals, vacuum integrals up to three loops and massless triangle integral families up to three loops are built into the `calc` setup. This includes also routines to perform the tensor decomposition. Additional work is necessary for the two-loop massless box topologies. In that case we use `tapir` [38] to generate two- loop massless box families onto which we map our scalar integrals. The IBP reduction is performed with `Kira` [39], where we reduce the scalar integrals to a set of master integrals. These are members of the two-loop massless box families introduced in ref. [40]. In a second step, these master integrals are rewritten as linear combinations of the canonical basis defined in refs. [41, 42], where they have also been calculated for the first time. We use the analytic results presented in ref. [40], consisting of 84 master integrals, plus crossings of external particles, in terms of a so-called "optimized functional basis" including logarithms, polylogarithms Li_n ($n = 2, 3, 4$) and $\mathrm{Li}_{2,2}$ functions. We note that the master integrals are only needed up to weight 3, so that the functions Li_4 and $\mathrm{Li}_{2,2}$ are not present in our final results. In addition, we

JHEP02(2026)191

perform a multivariate partial fractioning with the tool `MultivariateApart` [43] to simplify the complicated rational functions arising from these topologies. This reduces the size of the final expressions by a factor of 10 to 15.

2.2 UV renormalization and IR subtraction

The UV renormalization and IR subtraction closely follows ref. [37]. In particular, we renormalize the top-quark mass and the gluon wave function in the on-shell scheme and the strong coupling constant $\alpha_s^{(6)}$ in the $\overline{\text{MS}}$ scheme. In addition, we also need the decoupling constant of α_s to write the final results in terms of $\alpha_s^{(5)}$. A summary of all expressions can be found e.g. in ref. [44]. In the process $gg \to ZH$, γ_5 is present in the axial-vector coupling of the Z boson and in the pseudo-scalar coupling of the Goldstone boson. We adapt the prescription from ref. [45]. Thus, we have to renormalize the non-singlet axial-vector and pseudo-scalar currents with $Z^{ns} = Z_f^{ns} Z_{\overline{\text{MS}}}^{ns}$ and $Z^{ps} = Z_f^{ps} Z_{\overline{\text{MS}}}^{ps}$, respectively. The corresponding renormalization constants are given by [45, 46]

$$
\begin{aligned}
Z_f^{ns} &= 1 - 4a_s C_F + a_s^2 \left(22 C_F^2 - \frac{107}{9} C_A C_F + \frac{4}{9} C_F T_F n_f \right) , \\
Z_f^{ps} &= 1 - 8a_s C_F + a_s^2 \left(\frac{2}{9} C_A C_F + \frac{8}{9} C_F T_F n_f \right) ,
\end{aligned}
$$

and

$$
\begin{aligned}
Z_{\overline{\text{MS}}}^{ns} &= 1 + a_s^2 \left(\frac{22}{3\epsilon} C_A C_F - \frac{8}{3\epsilon} C_F T_F n_f \right) , \\
Z_{\overline{\text{MS}}}^{ps} &= 1 + a_s^2 \left(\frac{44}{3\epsilon} C_A C_F - \frac{16}{3\epsilon} C_F T_F n_f \right) ,
\end{aligned}
$$

with $C_A = 3$, $C_F = 4/3$, $T_F = 1/2$, $a_s = \alpha_s^{(6)}/(4\pi)$ and $n_f = n_h + n_l$, where $n_h = 1$ is the number of heavy quarks and $n_l = 5$ is the number of light quarks.

For the subtraction of IR singularities we follow refs. [47, 48], so that the finite form factors are given by

$$
\begin{aligned}
F^{(1),\text{fin}} &= F^{(1)} - \frac{1}{2} I_g^{(1)} F^{(0)}, \\
F^{(2),\text{fin}} &= F^{(2)} - \frac{1}{2} I_g^{(1)} F^{(1)} - \frac{1}{4} I_g^{(2)} F^{(0)},
\end{aligned}
\tag{2.5}
$$

where $I_g^{(1)}$ and $I_g^{(2)}$ are given e.g. in eqs. (20) to (24) in ref. [37] (see also ref. [48]).[2] $F^{(i)}$ are the coefficients of the renormalized form factors expanded in $\alpha_s^{(5)}$ as

$$
F = F^{(0)} + \frac{\alpha_s^{(5)}(\mu)}{\pi} F^{(1)} + \left(\frac{\alpha_s^{(5)}(\mu)}{\pi} \right)^2 F^{(2)} . \tag{2.6}
$$

[2] Note that there is a typo in eq. (24) of ref. [37] and eq. (13) or ref. [44]: in both cases the sign in front of the $C_A n_l$ colour structure should be a $(-)$ and not a $(+)$ sign.

JHEP02(2026)191

	T_F^3	$T_F^2 C_A$	$T_F^2 C_F$	$T_F\{C_A^2, C_A C_F, C_F^2\}$
F_{12}^+	$\mathcal{O}(1/m_t^0)$	$\mathcal{O}(1/m_t^0)$	$\mathcal{O}(1/m_t^0)$	$\mathcal{O}(1/m_t^0)$
F_{12}^-	$\mathcal{O}(1/m_t^0)$	$\mathcal{O}(1/m_t^0)$	$\mathcal{O}(1/m_t^0)$	$\mathcal{O}(1/m_t^4)$
F_2^-	$\mathcal{O}(1/m_t^0)$	$\mathcal{O}(1/m_t^0)$	$\mathcal{O}(1/m_t^0)$	$\mathcal{O}(1/m_t^4)$
F_3^+	–	$\mathcal{O}(1/m_t^0)$	$\mathcal{O}(1/m_t^2)$	$\mathcal{O}(1/m_t^4)$
F_3^-	–	$\mathcal{O}(1/m_t^0)$	$\mathcal{O}(1/m_t^2)$	$\star$
F_4	–	$\mathcal{O}(1/m_t^0)$	$\mathcal{O}(1/m_t^2)$	$\mathcal{O}(1/m_t^4)$

Table 1. The table entries show the lowest order of the large-mass expansion at which the different colour factors lead to non-zero contributions to the bare three-loop amplitude. The symbol "$-$" denotes that the colour factor vanishes exactly, while "$\star$" denotes that it is expected that the colour factor appears in higher-order expansion terms.

3 Renormalized virtual contribution

All form factors have been expanded up to $\mathcal{O}(1/m_t^4)$. We refrain from presenting explicit results for the individual form factors in this paper; our analytic ultra-violet renormalized results are available in a computer-readable form from ref. [49]. Furthermore, they are implemented in `ggxy`, see appendix. We provide both infra-red divergent and infra-red finite expressions. At one- and two-loop order we reproduce the results in the literature [20].

At one- and two-loop order several form factors start at order $1/m_t^4$. In particular, at one loop the form factor F_{12}^+ is the only one which starts at $\mathcal{O}(1/m_t^0)$, while all other form factors begin at $\mathcal{O}(1/m_t^4)$. F_3^- even vanishes completely. This situation differs only slightly at the two-loop level. The form factors F_{12}^- and F_2^- now also start at $\mathcal{O}(1/m_t^0)$ due to the one-particle reducible contributions (double-triangle diagrams), while the one-particle irreducible contributions still vanish at $\mathcal{O}(1/m_t^0)$ and $\mathcal{O}(1/m_t^2)$. Additionally, the form factor F_3^- no longer vanishes exactly but begins at $\mathcal{O}(1/m_t^6)$. On the other hand, at the three-loop level all six form factors have non-zero contributions at $\mathcal{O}(1/m_t^0)$, while several colour factors first appear at $\mathcal{O}(1/m_t^2)$ or $\mathcal{O}(1/m_t^4)$. An overview of the order in the large-mass expansion at which the different colour structures first contribute to the bare amplitude is given, for each of the six form factors, in table 1.

In the following we provide results for the squared amplitude which we define at LO, NLO and NNLO as follows

$$
\begin{aligned}
|A^{(0)}|^2 &= \frac{G_F^2 m_Z^2}{16 s^2} \sum_{\lambda_1,\lambda_2,\lambda_3} \left\{ \left[\tilde{A}^{(0),\mu\nu\rho}_{\text{sub}} \tilde{A}^{(0),\star,\mu'\nu'\rho'}_{\text{sub}} \right] \right\} \\
&\quad \times \varepsilon_{\lambda_1,\mu}(q_1)\, \varepsilon^\star_{\lambda_1,\mu'}(q_1)\, \varepsilon_{\lambda_2,\nu}(q_2)\, \varepsilon^\star_{\lambda_2,\nu'}(q_2)\, \varepsilon_{\lambda_3,\rho}(q_3)\, \varepsilon^\star_{\lambda_3,\rho'}(q_3)\,, \\
|A^{(1)}|^2 &= \frac{G_F^2 m_Z^2}{16 s^2} \sum_{\lambda_1,\lambda_2,\lambda_3} \left\{ 2\text{Re}\left[\tilde{A}^{(0),\mu\nu\rho}_{\text{sub}} \tilde{A}^{(1)\star,\mu'\nu'\rho'}_{\text{sub}} \right] \right\} \\
&\quad \times \varepsilon_{\lambda_1,\mu}(q_1)\, \varepsilon^\star_{\lambda_1,\mu'}(q_1)\, \varepsilon_{\lambda_2,\nu}(q_2)\, \varepsilon^\star_{\lambda_2,\nu'}(q_2)\, \varepsilon_{\lambda_3,\rho}(q_3)\, \varepsilon^\star_{\lambda_3,\rho'}(q_3)\,, \\
|A^{(2)}|^2 &= \frac{G_F^2 m_Z^2}{16 s^2} \sum_{\lambda_1,\lambda_2,\lambda_3} \left\{ 2\text{Re}\left[\tilde{A}^{(0),\mu\nu\rho}_{\text{sub}} \tilde{A}^{(2),\star,\mu'\nu'\rho'}_{\text{sub}} \right] + \left[\tilde{A}^{(1),\mu\nu\rho}_{\text{sub}} \tilde{A}^{(1),\star,\mu'\nu'\rho'}_{\text{sub}} \right] \right\}
\end{aligned}
$$

JHEP02(2026)191

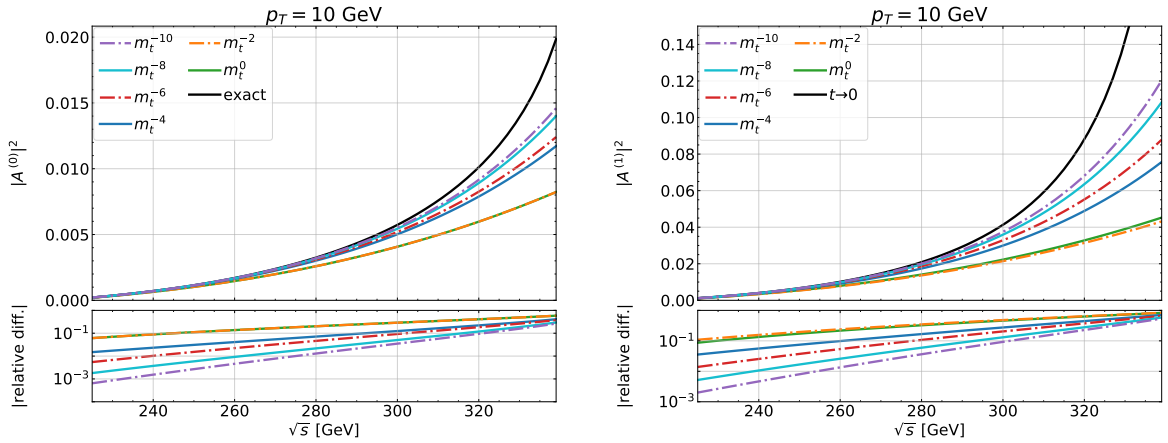

Figure 3. Squared amplitude at LO and NLO as a function of $\sqrt{s}$ for $p_T = 10\,\text{GeV}$, showing different expansion depths in $1/m_t^2$. Exact one-loop results and the results from the forward limit [21] at two loops are shown in black as a reference. The lower panel displays the relative difference to the reference values.

$$\times \varepsilon_{\lambda_1,\mu}(q_1)\, \varepsilon^{\star}_{\lambda_1,\mu'}(q_1)\, \varepsilon_{\lambda_2,\nu}(q_2)\, \varepsilon^{\star}_{\lambda_2,\nu'}(q_2)\, \varepsilon_{\lambda_3,\rho}(q_3)\, \varepsilon^{\star}_{\lambda_3,\rho'}(q_3)\,, \tag{3.1}$$

where $|A|^2$ has the same perturbative expansion as the form factors in eq. (2.6). $\tilde{A}^{(i)}_{\text{sub}}$ are the infrared-subtracted finite form factors evaluated for $\mu^2 = -s$, see also ref. [44]. In figure 3 we show results for $|A^{(0)}|^2$ and $|A^{(1)}|^2$ as a function of $\sqrt{s}$ for fixed transverse momentum $p_T = 10\,\text{GeV}$. In the upper panel we include, step-by-step, higher-order terms in $1/m_t^2$ up to $\mathcal{O}(1/m_t^{10})$. In addition, we display as reference values the exact results at one-loop order and the results from the expansion in the forward limit [21] at two loops, which approximates the exact result far below the percent level. In the lower panel the relative difference with respect to the reference results is shown.

A convergent behaviour of the large-m_t expansion can be expected only for $\sqrt{s}$ values below $2m_t$. This is indeed observed at LO. The $1/m_t^2$ terms vanish and we observe a relatively large jump once the $1/m_t^4$ terms are included. For $\sqrt{s} \lesssim 300\,\text{GeV}$ the contribution of higher $1/m_t^2$ terms is numerically less important. A similar pattern is observed at NLO, where again the $1/m_t^4$ terms provide a numerically large contribution.[3] Up to $\sqrt{s} \approx 300\,\text{GeV}$ the approximations including $1/m_t^4$ terms agree at the 10% level or better with the exact results.[4] We assume that this pattern of convergence extends to NNLO, which is our motivation to perform an expansion up to $1/m_t^4$. The computation of the next term in the $1/m_t$ expansion would be rather CPU-time expensive. The numerical results at NNLO up to $1/m_t^4$ are shown in figure 4, where we again find that the $\mathcal{O}(1/m_t^4)$ terms are numerically important.

In figure 5 we show LO, NLO and NNLO results for the squared amplitude, where we use $\alpha_s = 0.118$. In the left panel, only the infinite top quark mass results are included. We observe K factors at NLO and NNLO of 20% and 25%, respectively, which are almost independent of $\sqrt{s}$. In the right panel expansions up to $1/m_t^4$ are included in the calculation

[3] Both at LO and NLO we observe a pairing of an even and the subsequent odd expansion term in $1/m_t^2$; this has also been observed for $gg \to HH$ in ref. [50].

[4] We remark that after including $1/m_t^{10}$ terms at NLO, the difference reduces to about 3% for $\sqrt{s} = 300\,\text{GeV}$.

JHEP02(2026)191

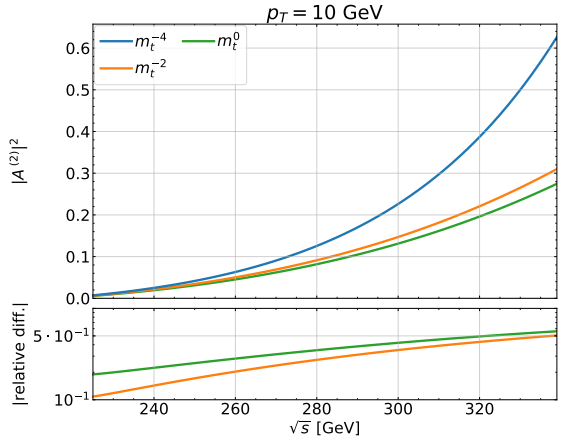

Figure 4. Squared amplitude at NNLO as a function of $\sqrt{s}$ for $p_T = 10\,\text{GeV}$, showing different expansion depths in $1/m_t^2$. In the lower panel the relative difference to the best available approximation $(1/m_t^4)$ is shown.

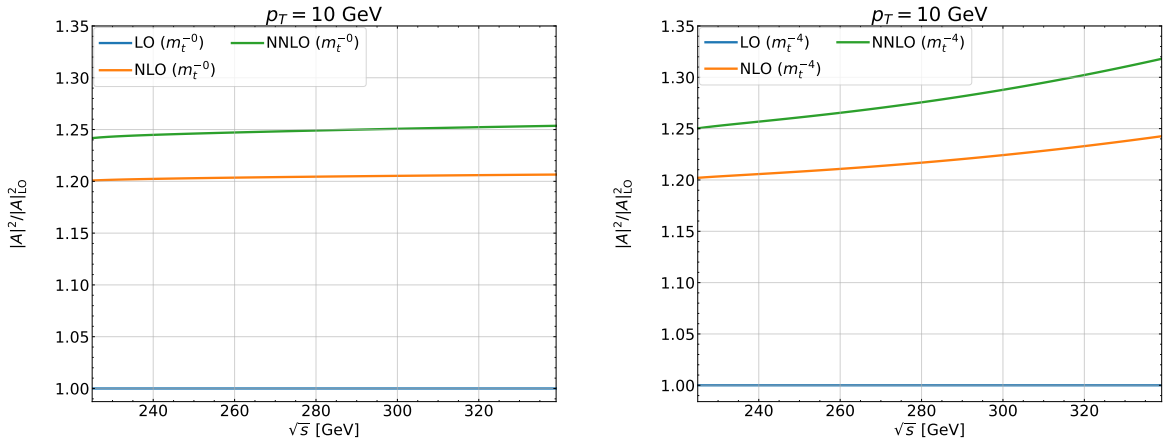

Figure 5. Squared amplitude at LO, NLO and NNLO as a function of $\sqrt{s}$ for $p_T = 10\,\text{GeV}$ normalized to the LO one. Left plot shows the results at the order $1/m_t^0$ and the right plot up to $1/m_t^4$.

of the form factors. Now we observe a slight increase on the K factors; at $\sqrt{s} = 300\,\text{GeV}$ they amount to about 22% and 28%.

4 Conclusions

We have computed the three-loop virtual corrections to $gg \to ZH$ in the large-m_t limit, taking into account triangle and box contributions. Furthermore, all one-particle irreducible and one-particle reducible diagrams are considered. This is necessary to obtain a finite result. We provide an expansion up to $1/m_t^4$. Since some of the form factors only start to contribute at $1/m_t^4$ we observe a relatively big contribution from this last expansion term. The leading term of our expansion provides an important ingredient for the construction of an approximate NNLO prediction in analogy to ref. [28] which is currently used for $gg \to HH$. The remaining terms constitute a benchmark result for future numerical calculations or

JHEP02(2026)191

expansions around other limits. Analytic results for all form factors can be found in ref. [49]. They are also implemented in the C++ library ggxy [29], which allows for a fast and convenient numerical evaluation. In particular, it is straightforward to generate the data for all plots shown in this paper.

Acknowledgments

This research was supported by the Deutsche Forschungsgemeinschaft (DFG, German Research Foundation) under grant 396021762 — TRR 257 "Particle Physics Phenomenology after the Higgs Discovery". The work of J. D. was supported by STFC Consolidated Grant ST/X000699/1. The research of K. S. was funded by the European Union's Horizon Research and Innovation Program under the Marie Skłodowska-Curie grant agreement No. 101204018.

A Implementation in ggxy

All six form factors of eq. (2.4) are implemented in ggxy, which can be obtained from https://gitlab.com/ggxy/ggxy-release. In particular, we include terms up to m_t^{-10} at one- and two-loop and terms up to m_t^{-4} at three-loop order. The finite part of the form factors at the different loop-orders can be evaluated using the functions in the header files ff/ggzh/LMEggzh{1,2,3}lFF.h,

```
complex<double> LMEggzh{1,2,3}l<FF>(double s, double t,
                                    double mzs, double mhs,
                                    double mts, double mus,
                                    bool irsubtr = true,
                                    unsigned ExpDepth = {5,5,2});
```

or

```
vector<complex<double>> LMEggzh{1,2,3}l<FF>imts(double s, double t,
                                                double mzs, double mhs,
                                                double mts, double mus,
                                                bool irsubtr = true);
```

where <FF> is a placeholder for the six form factors which are abbreviated as FF12p, FF12m, FF2m, FF3p, FF3m and FF4. The return value is either the form factor up to the order ExpDepth in the $1/m_t^2$ expansion, where the default values correspond to highest number of implemented expansion terms, or a vector containing the coefficients of the expansion. The parameter mus defines the squared renormalization scale (μ^2) and irsubtr is used to (de-)activate the IR subtraction of the two- and three-loop form factors. An example for the numerical evaluation of the form factors is given in the file ff-lme.cpp which can be found in the path examples/ggzh-FF. The example program evaluates the form factors for the phase-space region shown in the main text, where a typical agreement of six digits is found with respect to the evaluation with Mathematica.

Alternatively, the squared amplitudes of eq. (3.1) can also be directly computed with the function

JHEP02(2026)191

```
vector<double> ggzh3lAsq(double s, double t, double mzs,
                         double mhs, double mts, double GF,
                         int ExpDepth = -1);
```

defined in the header file `ff/ggzh/ggzhFF.h`, where `GF` denotes G_F and `ExpDepth` defines again the number of expansion terms in the $1/m_t^2$ expansion but the default value is set to `ExpDepth = -1`, which corresponds to the case where at each loop-order all possible expansion terms are taken into account. Internally this function computes the squared amplitude by performing the summation over the helicity amplitudes, which are calculated with the function

```
vector<complex<double>> ggZHhels(vector<complex<double>> FF,
                                 double s, double t, double mzs,
                                 double mhs);
```

where the input vector `FF` is assumed to contain the form factors in the ordering of equation (2.4) and returns the helicity amplitudes $\mathcal{A}_{+++}$, $\mathcal{A}_{++-}$, $\mathcal{A}_{++0}$, $\mathcal{A}_{+-+}$, $\mathcal{A}_{+--}$, $\mathcal{A}_{+-0}$. The polarization vectors of the gluons and the Z boson are chosen as in ref. [21]. An example for the evaluation of the squared amplitude is given in the file `examples/ggzh-nnlo/Asq-lme.cpp`, which in combination with the python scripts in the same directory reproduces figure 4 and 5.

Data Availability Statement. This article has associated data in a data repository. Available at https://www.ttp.kit.edu/preprints/2025/ttp25-047.

Code Availability Statement. This article has no associated code or the code will not be deposited.

References

[1] ATLAS collaboration, *Observation of $H \to b\bar{b}$ decays and VH production with the ATLAS detector*, *Phys. Lett. B* **786** (2018) 59 [arXiv:1808.08238] [INSPIRE].

[2] CMS collaboration, *Observation of Higgs boson decay to bottom quarks*, *Phys. Rev. Lett.* **121** (2018) 121801 [arXiv:1808.08242] [INSPIRE].

[3] ATLAS collaboration, *Study of High-Transverse-Momentum Higgs Boson Production in Association with a Vector Boson in the qqbb Final State with the ATLAS Detector*, *Phys. Rev. Lett.* **132** (2024) 131802 [arXiv:2312.07605] [INSPIRE].

[4] T. Han and S. Willenbrock, *QCD Correction to the $pp \to WH$ and ZH Total Cross Sections*, *Phys. Lett. B* **273** (1991) 167 [INSPIRE].

[5] O. Brein, A. Djouadi and R. Harlander, *NNLO QCD corrections to the Higgs-strahlung processes at hadron colliders*, *Phys. Lett. B* **579** (2004) 149 [hep-ph/0307206] [INSPIRE].

[6] J. Baglio, C. Duhr, B. Mistlberger and R. Szafron, *Inclusive production cross sections at N^3LO*, *JHEP* **12** (2022) 066 [arXiv:2209.06138] [INSPIRE].

JHEP02(2026)191

[7] O. Brein, R.V. Harlander and T.J.E. Zirke, *vh@nnlo — Higgs Strahlung at hadron colliders*, *Comput. Phys. Commun.* **184** (2013) 998 [arXiv:1210.5347] [INSPIRE].

[8] R.V. Harlander, J. Klappert, S. Liebler and L. Simon, *vh@nnlo-v2: New physics in Higgs Strahlung*, *JHEP* **05** (2018) 089 [arXiv:1802.04817] [INSPIRE].

[9] G. Ferrera, M. Grazzini and F. Tramontano, *Associated ZH production at hadron colliders: the fully differential NNLO QCD calculation*, *Phys. Lett. B* **740** (2015) 51 [arXiv:1407.4747] [INSPIRE].

[10] J.M. Campbell, R.K. Ellis and C. Williams, *Associated production of a Higgs boson at NNLO*, *JHEP* **06** (2016) 179 [arXiv:1601.00658] [INSPIRE].

[11] M.L. Ciccolini, S. Dittmaier and M. Kramer, *Electroweak radiative corrections to associated WH and ZH production at hadron colliders*, *Phys. Rev. D* **68** (2003) 073003 [hep-ph/0306234] [INSPIRE].

[12] A. Denner, S. Dittmaier, S. Kallweit and A. Muck, *Electroweak corrections to Higgs-strahlung off W/Z bosons at the Tevatron and the LHC with HAWK*, *JHEP* **03** (2012) 075 [arXiv:1112.5142] [INSPIRE].

[13] A. Denner, S. Dittmaier, S. Kallweit and A. Mück, *HAWK 2.0: A Monte Carlo program for Higgs production in vector-boson fusion and Higgs strahlung at hadron colliders*, *Comput. Phys. Commun.* **195** (2015) 161 [arXiv:1412.5390] [INSPIRE].

[14] D.A. Dicus and C. Kao, *Higgs Boson — Z^0 Production From Gluon Fusion*, *Phys. Rev. D* **38** (1988) 1008 [*Erratum ibid.* **42** (1990) 2412] [INSPIRE].

[15] B.A. Kniehl, *Associated Production of Higgs and Z Bosons From Gluon Fusion in Hadron Collisions*, *Phys. Rev. D* **42** (1990) 2253 [INSPIRE].

[16] LHC Higgs Cross Section Working Group collaboration, *Handbook of LHC Higgs Cross Sections: 4. Deciphering the Nature of the Higgs Sector*, *CERN Yellow Rep. Monogr.* **2** (2017) 1 [arXiv:1610.07922] [INSPIRE].

[17] C. Englert, M. McCullough and M. Spannowsky, *Gluon-initiated associated production boosts Higgs physics*, *Phys. Rev. D* **89** (2014) 013013 [arXiv:1310.4828] [INSPIRE].

[18] L. Altenkamp et al., *Gluon-induced Higgs-strahlung at next-to-leading order QCD*, *JHEP* **02** (2013) 078 [arXiv:1211.5015] [INSPIRE].

[19] A. Hasselhuhn, T. Luthe and M. Steinhauser, *On top quark mass effects to $gg \to ZH$ at NLO*, *JHEP* **01** (2017) 073 [arXiv:1611.05881] [INSPIRE].

[20] J. Davies, G. Mishima and M. Steinhauser, *Virtual corrections to $gg \to ZH$ in the high-energy and large-m_t limits*, *JHEP* **03** (2021) 034 [arXiv:2011.12314] [INSPIRE].

[21] J. Davies et al., *Two-loop QCD corrections to ZH and off-shell Z boson pair production in gluon fusion*, arXiv:2509.07072 [INSPIRE].

[22] L. Alasfar et al., *Virtual corrections to $gg \to ZH$ via a transverse momentum expansion*, *JHEP* **05** (2021) 168 [arXiv:2103.06225] [INSPIRE].

[23] L. Chen et al., *ZH production in gluon fusion: two-loop amplitudes with full top quark mass dependence*, *JHEP* **03** (2021) 125 [arXiv:2011.12325] [INSPIRE].

[24] G. Wang, X. Xu, Y. Xu and L.L. Yang, *Next-to-leading order corrections for $gg \to ZH$ with top quark mass dependence*, *Phys. Lett. B* **829** (2022) 137087 [arXiv:2107.08206] [INSPIRE].

[25] L. Chen et al., *ZH production in gluon fusion at NLO in QCD*, *JHEP* **08** (2022) 056 [arXiv:2204.05225] [INSPIRE].

JHEP02(2026)191

[26] G. Degrassi, R. Gröber, M. Vitti and X. Zhao, *On the NLO QCD corrections to gluon-initiated ZH production*, *JHEP* **08** (2022) 009 [arXiv:2205.02769] [INSPIRE].

[27] B. Campillo Aveleira et al., *$gg \to ZH$: updated predictions at NLO QCD*, arXiv:2508.09905 [DOI:10.21468/SciPostPhysCommRep.16] [INSPIRE].

[28] M. Grazzini et al., *Higgs boson pair production at NNLO with top quark mass effects*, *JHEP* **05** (2018) 059 [arXiv:1803.02463] [INSPIRE].

[29] J. Davies, K. Schönwald, M. Steinhauser and D. Stremmer, *ggxy: A flexible library to compute gluon-induced cross sections*, *Comput. Phys. Commun.* **320** (2026) 109933 [arXiv:2506.04323] [INSPIRE].

[30] L. Bündgen, R.V. Harlander, S.Y. Klein and M.C. Schaaf, *FeynGame 3.0*, *Comput. Phys. Commun.* **314** (2025) 109662 [arXiv:2501.04651] [INSPIRE].

[31] P. Nogueira, *Automatic Feynman Graph Generation*, *J. Comput. Phys.* **105** (1993) 279 [INSPIRE].

[32] B. Ruijl, T. Ueda and J. Vermaseren, *FORM version 4.2*, arXiv:1707.06453 [INSPIRE].

[33] R. Harlander, T. Seidensticker and M. Steinhauser, *Complete corrections of Order alpha alpha-s to the decay of the Z boson into bottom quarks*, *Phys. Lett. B* **426** (1998) 125 [hep-ph/9712228] [INSPIRE].

[34] T. Seidensticker, *Automatic application of successive asymptotic expansions of Feynman diagrams*, in the proceedings of the *6th International Workshop on New Computing Techniques in Physics Research: Software Engineering, Artificial Intelligence Neural Nets, Genetic Algorithms, Symbolic Algebra, Automatic Calculation*, Heraklion, Greece, April 12–16 (1999) [hep-ph/9905298] [INSPIRE].

[35] V.A. Smirnov, *Applied asymptotic expansions in momenta and masses*, *Springer Tracts Mod. Phys.* **177** (2002) 1 [INSPIRE].

[36] R.K. Ellis and G. Zanderighi, *Scalar one-loop integrals for QCD*, *JHEP* **02** (2008) 002 [arXiv:0712.1851] [INSPIRE].

[37] J. Davies and M. Steinhauser, *Three-loop form factors for Higgs boson pair production in the large top mass limit*, *JHEP* **10** (2019) 166 [arXiv:1909.01361] [INSPIRE].

[38] M. Gerlach, F. Herren and M. Lang, *tapir: A tool for topologies, amplitudes, partial fraction decomposition and input for reductions*, *Comput. Phys. Commun.* **282** (2023) 108544 [arXiv:2201.05618] [INSPIRE].

[39] J. Klappert, F. Lange, P. Maierhöfer and J. Usovitsch, *Integral reduction with Kira 2.0 and finite field methods*, *Comput. Phys. Commun.* **266** (2021) 108024 [arXiv:2008.06494] [INSPIRE].

[40] T. Gehrmann, A. von Manteuffel and L. Tancredi, *The two-loop helicity amplitudes for $q\bar{q}' \to V_1V_2 \to 4$ leptons*, *JHEP* **09** (2015) 128 [arXiv:1503.04812] [INSPIRE].

[41] J.M. Henn, K. Melnikov and V.A. Smirnov, *Two-loop planar master integrals for the production of off-shell vector bosons in hadron collisions*, *JHEP* **05** (2014) 090 [arXiv:1402.7078] [INSPIRE].

[42] F. Caola, J.M. Henn, K. Melnikov and V.A. Smirnov, *Non-planar master integrals for the production of two off-shell vector bosons in collisions of massless partons*, *JHEP* **09** (2014) 043 [arXiv:1404.5590] [INSPIRE].

[43] M. Heller and A. von Manteuffel, *MultivariateApart: Generalized partial fractions*, *Comput. Phys. Commun.* **271** (2022) 108174 [arXiv:2101.08283] [INSPIRE].

JHEP02(2026)191

[44] J. Davies, K. Schönwald and M. Steinhauser, *Three-loop large-N_c virtual corrections to $gg \to HH$ in the forward limit*, *JHEP* **08** (2025) 192 [arXiv:2503.17449] [INSPIRE].

[45] S.A. Larin, *The Renormalization of the axial anomaly in dimensional regularization*, *Phys. Lett. B* **303** (1993) 113 [hep-ph/9302240] [INSPIRE].

[46] L. Chen, M. Czakon and M. Niggetiedt, *Renormalization of the pseudoscalar operator at four loops in QCD*, *JHEP* **12** (2024) 045 [arXiv:2410.18674] [INSPIRE].

[47] S. Catani, *The singular behavior of QCD amplitudes at two loop order*, *Phys. Lett. B* **427** (1998) 161 [hep-ph/9802439] [INSPIRE].

[48] D. de Florian and J. Mazzitelli, *A next-to-next-to-leading order calculation of soft-virtual cross sections*, *JHEP* **12** (2012) 088 [arXiv:1209.0673] [INSPIRE].

[49] J. Davies, D. Grau, K. Schoenwald, M. Steinhauser and D. Stremmer, *TTP25-047 Three-loop corrections to $gg \to ZH$ in the large top quark mass limit*, https://www.ttp.kit.edu/preprints/2025/ttp25-047.

[50] J. Grigo, J. Hoff, K. Melnikov and M. Steinhauser, *On the Higgs boson pair production at the LHC*, *Nucl. Phys. B* **875** (2013) 1 [arXiv:1305.7340] [INSPIRE].

JHEP02(2026)191